T-matrix approach to equilibium and nonequilibrium carrier-carrier scattering in semiconductors

D. O. Gericke, S. Kosse, and M. Schlanges
Institut für Physik, Ernst-Moritz-Arndt Universität Greifswald, Domstrasse 10a, 17487 Greifswald, Germany

M. Bonitz
FB Physik, Universität Rostock, Universitätsplatz 3, 18051 Rostock, Germany
(Received 24 July 1998; revised manuscript received 27 October 1998)

An analysis of strong-coupling effects in carrier-carrier scattering in electron-hole plasmas in semiconductors is presented. The conventional approach to scattering and dephasing rates is based on the Born approximation (a scattering cross section proportional to the square of the dynamically screened interaction potential), and is strictly valid only in the limit of the weakly coupled quantum plasma. Otherwise, strong correlations are expected to become important in the scattering quantities. Therefore, we perform a thorough analysis of scattering rates in the framework of the statically screened *T*-matrix (ladder) approximation. We solve the two-particle Schrödinger equation and provide explicit results for the carrier-carrier scattering rates in equilibrium as well as for optical excitation conditions. Numerical results for GaAs show evidence of significant deviations from the common Born approximation. Finally, dynamic screening effects are included approximately. [S0163-1829(99)01815-9]

I. INTRODUCTION

Recent impressive progress in the subpicosecond spectroscopy of electron-hole (e-h) plasmas in semiconductors has made time-resolved high-precision optical measurements possible[1] which allow one to study the influence of carrier-carrier scattering; see, e.g., Refs. 2 and 3. Similar progress is observed in the field of semiconductor transport; for a recent overview, cf. Ref. 4. This increased the need for a high-quality theoretical modeling of the nonequilibrium properties of charge carriers in semiconductors, including the relevant scattering and dephasing mechanisms, which has to be based on kinetic equations such as the Boltzmann equation[5–7] or its interband extension, the semiconductor Bloch equations.[8,9] Among the various scattering processes, carrier-carrier scattering plays a central role, and is expected to dominate in high-quality samples and at temperatures below the phonon threshold.

The commonly used carrier-carrier scattering models are characterized by (i) an approximation of the differential scattering cross sections (scattering probabilities) by the square of the dynamically screened binary interaction potential, $\sigma_{ab} \sim |V_{ab}^S|^2$; and (ii) a Markovian form of the scattering integrals. Strictly speaking, this confines the applicability of these models (i) to the case of weak carrier-carrier interaction (see Fig. 1), and (ii) to sufficiently long times ($t > \tau_{\rm cor}$, where $\tau_{\rm cor}$ is the correlation time of the system,[10] which is of the order of the inverse plasma frequency[11]). While the second aspect has been intensively studied in the context of so-called memory effects in recent years,[4,9,12–15] the first has attracted much less attention.[16–18] In particular, it remains widely unclear how important strong-coupling effects (effects beyond the Born approximation) are for the relaxation of a nonequilibrium carrier ensemble in semiconductors.

Strong-coupling effects in two-particle scattering have been intensively studied in various fields, including nuclear matter[19] and dense plasmas.[20,21] However, despite remarkable theoretical work,[22–24] a thorough quantitative investigation for semiconductors which applies to general nonequilibrium situations is still missing. The theoretical approach has to be based upon a summation of the full Born series (ladder series) which yields the *T*-matrix approximation.[21,23,25] To analyze the relevance of these effects, it is useful to consider

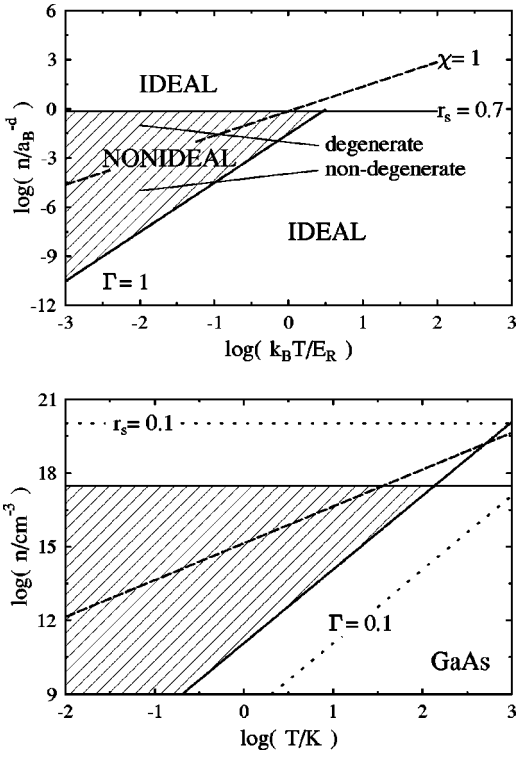

FIG. 1. Strong-coupling region in equilibrium. n-T plane in system-independent dimensionless parameters (d is the dimensionality) and for electrons in a bulk semiconductor (GaAs) (upper and lower figure, respectively).

the dimensionless parameters Γ (coupling parameter), r_s (Brueckner parameter), and χ (degeneracy parameter):[20]

$$\Gamma_a \equiv \frac{|\langle V_{aa}\rangle|}{\langle T_a\rangle} \rightarrow \frac{l}{\bar{r}} = \frac{4\pi e_a^2}{\epsilon_B k_B T}\frac{1}{\bar{r}}, \tag{1}$$

$$r_s \equiv \frac{\bar{r}}{a_B}, \tag{2}$$

$$\chi_a \equiv \frac{n_a \Lambda_a^3}{2s_a+1}, \quad \Lambda_a = \sqrt{\frac{2\pi\hbar^2}{m_a k_B T}}. \tag{3}$$

Γ_a is essentially the ratio of the mean potential to the kinetic energy of particles of species ''a,'' which, in the classical case, is equivalent to the ratio of the Landau length l to the mean interparticle distance $\bar{r}$ (e_a is the charge and ϵ_B the background dielectric constant). Furthermore, r_s is the ratio of the interparticle distance to the Bohr radius of bound states (excitons), and $\chi^{1/3}$ is essentially the ratio of the thermal (DeBroglie) wavelength Λ_a to the interparticle distance (s_a is the spin projection). Now the general prediction is that T-matrix effects are important in the so-called corner of correlations,[21] where the mean correlation energy of the carriers is comparable to or even larger than their mean kinetic energy. In equilibrium, a reasonable estimate to the boundaries of this region in the density-temperature plane is given by the lines[21]

$$\Gamma_a = 1 \quad \text{and} \quad r_s = 0.7, \tag{4}$$

which are shown in Fig. 1 for an electron plasma in d dimensions (upper figure) and for bulk GaAs (lower figure). While the first condition of Eq. (4) gives the low-density limit (classical plasma), the second applies to the high-density case (quantum plasma). Conversely, the commonly used Born approximation may be expected to be applicable only well outside this region, although it is well known that even there it does not necessarily possess the correct limiting behavior. In particular, the low-density (classical) limit of the Born approximation deviates from the exact asymptotic result (for example, from the Spitzer result for the conductivity) which is reproduced only from the T-matrix approximation; see, e.g., Ref. 21). In fact, our numerical investigations show that this is also the case for low-density electron-hole plasmas, which is a further strong motivation to study carrier-carrier scattering in the T-matrix approximation.

However, these are rather general predictions which require a reliable quantitative verification. This is the intention of our investigation, which continues our previous work on T-matrix effects in equilibrium.[26] In this paper, we study strong-coupling effects in carrier-carrier scattering in more detail, both in equilibrium and nonequilibrium, concentrating on bulk material (choosing GaAs as an example) and using a two-band model. We limit ourselves to nondegenerate electron-hole plasmas ($\chi<1$), which allows us to advance into the shaded region in Fig. 1 making use of efficient phase shift techniques.[27,28] Although for $\chi>1$ one does not expect a qualitatively different behavior (an estimate of degeneracy effects is given in Sec. IV), here one is forced to perform computationally costly solutions of the Lippmann-Schwinger equation.[29] Moreover, this approach is, so far, feasible only in equilibrium.

This paper is organized as follows. In Sec. II A, we give a brief summary of the quantum kinetic description of optical and transport processes in semiconductors, focusing on the influence of (incoherent) carrier scattering and dephasing contributions in the common Born approximation. Section II B gives a general discussion of the T-matrix approximation for the scattering rates. Next, in Sec. II C, we derive explicit results for the equilibrium and nonequilibrium scattering rates for bulk semiconductors with an isotropic momentum distribution. Section III contains numerical results for the cross sections and scattering rates for equilibrium as well as nonequilibrium situations. Section IV concludes our paper with an analysis of the limitations of the used approximation. In particular, the incorporation of dynamical screening effects into the T matrices is discussed, and results are presented.

II. THEORETICAL CONCEPTS

A. Interband quantum kinetic equations

We briefly recall the kinetic equations for a description of optical and transport phenomena in semiconductors. Following the notation of Kadanoff and Baym,[25] we define the one-particle two-time correlation functions as fermionic field operators averages $g^{<}_{\mu_1\mu_2}(kt_1t_2) = -(1/i\hbar)\langle \psi^{\dagger}_{\mu_2 k}(t_2)\, \psi_{\mu_1 k}(t_1)\rangle$ and $g^{>}_{\mu_1\mu_2}(kt_1t_2) = (1/i\hbar)\langle \psi_{\mu_1 k}(t_1)\, \psi^{\dagger}_{\mu_2 k}(t_2)\rangle$, where μ_1 and μ_2 label the energy bands (or subbands). The equal time limit $g^{<}_{\mu_1\mu_2}(tt) = -i\hbar f_{\mu_1\mu_2}(t)$ defines the Wigner distributions f (for $\mu_1=\mu_2$) and the transition probabilities (interband polarizations) P (for $\mu_1\neq\mu_2$). In the presence of an electromagnetic field, $g^{\gtrless}$ evolve according to the interband Kadanoff–Baym equations (two–time semiconductor Bloch equations; see, e.g., Refs. 4 and 9) which, in the spatially homogeneous case, read

$$\left\{ i\hbar\frac{\partial}{\partial t_1} - \epsilon_{\mu_1}(\tilde{\mathbf{k}}_1)\right\} g^{\gtrless}_{\mu_1\mu_2}(\mathbf{k}t_1t_2) - \sum_{\bar{\mu}} \Sigma^{\mathrm{HF}}_{\mu_1\bar{\mu}}(\mathbf{k}t_1) g^{\gtrless}_{\bar{\mu}\mu_2}(\mathbf{k}t_1t_2) = I^{\gtrless}_{\mu_1\mu_2}(\mathbf{k}t_1t_2), \tag{5}$$

where ϵ_μ is the one-particle energy for band (component) μ, $\tilde{\mathbf{k}}_\mu = \mathbf{k} - (e_\mu/c\hbar)\mathbf{A}$, Σ^{HF} is the Hartree-Fock self energy, and $\mathbf{A}(t)$ the vector potential which obeys Maxwell's equations.

While the left-hand side of Eq. (5) describes mean-field phenomena, collective and coherent excitonic effects, the collision integrals $I^{\gtrless}$ on the right-hand side (the general definition can be found in textbooks; see, e.g., Ref. 4) contains the influence of scattering (correlations). $I^{\gtrless}$ govern the dephasing of the interband polarization as well as the transport properties of the

material, including the relaxation time τ_R of the carrier distributions, the carrier mobility, the conductivity, and so on. In this paper, we consider in detail incoherent effects caused by carrier scattering.

The Kadanoff-Baym equations (5) can be solved directly,[14,30] or may serve as the starting point to derive equations of motion for the Wigner functions and interband polarizations, i.e., the semiconductor Bloch equations

$$\left\{\frac{\partial}{\partial T}+i\frac{\epsilon_{\mu_1}(\tilde{\mathbf{k}})-\epsilon_{\mu_2}(\tilde{\mathbf{k}})}{\hbar}\right\}f_{\mu_1\mu_2}(T)-\sum_{\mu}\{\Sigma^{\mathrm{HF}}_{\mu_1\bar{\mu}}(T)f_{\bar{\mu}\mu_2}(T)-f_{\mu_1\bar{\mu}}(T)\Sigma^{\mathrm{HF}}_{\bar{\mu}\mu_2}(T)\}=I_{\mu_1\mu_2}(T),$$

$$I_{\mu_1\mu_2}(T)=\hbar\sum_{\mu}\int_{-\infty}^{T}d\bar{t}\,[\Sigma^{>}_{\mu_1\bar{\mu}}(T\bar{t})\,g^{<}_{\bar{\mu}\mu_2}(\bar{t}T)-\Sigma^{<}_{\mu_1\bar{\mu}}(T\bar{t})\,g^{>}_{\bar{\mu}\mu_2}(\bar{t}T)-g^{>}_{\mu_1\bar{\mu}}(T\bar{t})\,\Sigma^{<}_{\bar{\mu}\mu_2}(\bar{t}T)+g^{<}_{\mu_1\bar{\mu}}(T\bar{t})\,\Sigma^{>}_{\bar{\mu}\mu_2}(\bar{t}T)], \quad (6)$$

where T is the macroscopic time $T=(t_1+t_2)/2$, and $\Sigma^{\gtrless}$ are generalized scattering rates (self-energies). The momentum argument in f, I, g, and Σ has been suppressed. To come to a closed equation for $f_{\mu_1\mu_2}(T)$, one has to solve two problems concerning the collision integral which were mentioned in the Sec. I: (i) suitable approximations for the self energy have to be given, and (ii) the two-time functions have to be expressed in terms of f and P. Since our main interest in this paper is the derivation and critical test of improved expressions for the carrier self-energy, we use the simple Kadanoff-Baym ansatz[25] to solve problem (ii) and neglect the influence of the interband propagators.[31–33] Furthermore, to simplify the analysis of T-matrix effects, we concentrate in the following on the band-diagonal self-energies. Below, we will change to the electron-hole picture using latin subscripts to label the carrier species, i.e., $\Sigma_{\mu\mu}\to\Sigma_a$. Thus Σ_a includes electron-electron, hole-hole, and electron-hole scattering, while polarization scattering is neglected. As a result, we obtain for the band-diagonal collision terms in Eq. (6)

$$I_a(kT)=i\Sigma^{<}_a(kT,\hbar\omega=\epsilon_a(k))\,[1-f_a(kT)]-i\Sigma^{>}_a(kT,\hbar\omega=\epsilon_a(k))\,f_a(kT), \quad (7)$$

which involve the well-known Markovian (''on-shell,'' i.e., kinetic energy conserving) scattering rates $\Sigma^{\gtrless}_a$. We mention that $i\Sigma^{\gtrless}_a(k)$ are positive real quantities which have the meaning of probabilities of scattering ''into'' and ''out of'' state k, which are being multiplied in Eq. (7) by the probabilities that the state is empty $(1-f)$ or occupied (f), respectively.

Carrier-carrier scattering in semiconductors has been investigated so far mainly in the frame of weak-coupling approximations. This leads to the Born approximation for the self-energy,

$$i\Sigma^{\gtrless}_a(k_1,T)=\sum_b\sum_{k_2\bar{k}_1\bar{k}_2}|V^S_{ab}(k_1-\bar{k}_1,\epsilon_1-\bar{\epsilon}_1,T)|^2\delta_{k_1+k_2,\bar{k}_1+\bar{k}_2}2\pi\delta(\epsilon_1+\epsilon_2-\bar{\epsilon}_1-\bar{\epsilon}_2)f^{\gtrless}_a(\bar{k}_1,T)f^{\gtrless}_b(\bar{k}_2,T)f^{\lessgtr}_b(k_2,T)$$
$$+(\text{exchange}), \quad (8)$$

where we used the short notation $f^{<}_a\equiv f_a$ and $f^{>}_a\equiv 1-f_a$. Here $V^S_{ab}(k,\omega,T)=V_{ab}(k)/\epsilon^R(k,\omega,T)$ is the dynamically screened Coulomb potential in the random-phase approximation (RPA) with the retarded dielectric function $\epsilon^R(k,\omega,T)=1-\Sigma_a V_{aa}(k)\Pi^R_a(k,\omega,T)$, and nonequilibrium intraband polarization function Π^R, which accounts for the influence of collective plasma excitations on the scattering process;[5] see also Refs. 34 and 35.

To avoid the numerically difficult evaluation of the dynamically screened potential,[5] often the (quasi-)static long-wavelength limit of the RPA dielectric function is used which, in three dimensions, is given by[34] $\epsilon^R(k,T)=1-\kappa^2(T)/k^2$, and, correspondingly,

$$V^S_{ab}(k,T)=\frac{4\pi e_a e_b/\epsilon_B}{k^2+\kappa^2(T)}$$

with

$$\kappa^2(T)=\frac{2}{\hbar^2\pi\epsilon_B}\sum_a e_a^2 m_a\int_0^\infty dK\,f_a(K,T). \quad (9)$$

The Born approximation (8) together with Eq. (9), will be used below in most of the numerical comparisons with the T-matrix results. The influence of dynamical screening and its combination with strong-coupling effects will be discussed in Sec. IV.

B. *T*-matrix carrier-carrier scattering rates

As pointed out in Sec. I, the properties of strongly correlated plasmas are essentially influenced by multiple scattering and bound states. In order to include these effects one has to go beyond the Born approximation (8), summing up higher-order ladder diagrams. The full two-particle ladder sum yields the scattering rates in binary collision approximation, the general nonequilibrium definition of which is[25,36,37] (we substitute $\Sigma_{\mathbf{k}}\to(V/(2\pi\hbar)^3)\int d\mathbf{p}$),

$$i\Sigma^{\gtrless}_a(\mathbf{p}_a,tt')$$
$$=\hbar\sum_b\int\frac{d\mathbf{p}_b}{(2\pi\hbar)^3}\langle\mathbf{p}_a\mathbf{p}_b|T^{\gtrless}_{ab}(tt')|\mathbf{p}_b\mathbf{p}_a\rangle\,g^{\lessgtr}_b(\mathbf{p}_b,t't), \quad (10)$$

where T_{ab} is the T matrix. Since we consider fermionic particles (electrons and holes), the anti-symmetrized T matrix has to be used in the case of identical scatterers $(a=b)$.

The T-matrix approach is a well-developed concept of many-particle theory to describe strong dynamic correlations, especially in nuclear physics and plasma theory, but it has been applied less to semiconductors. Therefore, before explicitly calculating the scattering rates, it is useful to give a brief discussion of important relations of the binary collision approximation. The T matrices are defined by the two-time two-particle correlation functions $G_{ab}^{\gtrless}$ in the particle-particle channel,

$$T_{ab}^{\gtrless}(t,t') = i\, V_{ab}^{S}\, G_{ab}^{\gtrless}(t,t')\, V_{ab}^{S}, \tag{11}$$

where $G_{ab}^{\gtrless}(t,t')$ describe the behavior of a particle pair in an interacting many-particle system (for the definition, see Refs. 25). V_{ab}^{S} is the screened potential for which we use the static limit (9). Thus the central problem is the determination of the binary correlation functions $G_{ab}^{\gtrless}$.

An efficient approach is to express the two-particle correlation functions as a bilinear expansion in terms of the wave functions of the interacting particle pair $|\Psi_K\rangle$.[38] Then, Fourier transforming $G_{ab}^{\gtrless}$ with respect to the microscopic time $t-t'$ and using the local approximation, we obtain

$$G_{ab}^{\gtrless}(\omega,T) = \sum_K |\Psi_K\rangle\langle\Psi_K|\, F_K^{\gtrless}(T)\, 2\pi\delta(\hbar\omega - E_K). \tag{12}$$

The sum in Eq. (12) runs over all possible bound and scattering states, with $F_K^{\gtrless}$ being the corresponding occupation numbers. The two-particle states $|\Psi_K\rangle$ and the energy eigenvalues E_K follow from an effective Schrödinger equation which, in momentum representation, reads

$$[E_K - \epsilon_a(p_a) - \epsilon_b(p_b)]\langle \mathbf{p}_a\mathbf{p}_b|\Psi_K\rangle - [1 - f_a(\mathbf{p}_a) - f_b(\mathbf{p}_b)] \int \frac{d\overline{\mathbf{p}}_a}{(2\pi\hbar)^3}\frac{d\overline{\mathbf{p}}_b}{(2\pi\hbar)^3}\langle \mathbf{p}_a\mathbf{p}_b|V_{ab}^{S}|\overline{\mathbf{p}}_b\overline{\mathbf{p}}_a\rangle\langle\overline{\mathbf{p}}_a\overline{\mathbf{p}}_b|\Psi_K\rangle = 0. \tag{13}$$

This is a generalization of the usual two-particle Schrödinger equation which accounts for the influence of the surrounding particles on the pair a-b: first, the one-particle energies are modified, $\epsilon_a(p) = \epsilon_a^0(p) + \Delta_a$; and second, the interaction potential is replaced by the statically screened Coulomb potential V_{ab}^{S}. For consistency of the approximation scheme, the energy shifts are approximated by $\Delta_a = -\kappa e_a^2/2\epsilon_B$.[21,24] It should be noted that Eq. (13) is not Hermitian, which requires a second Schrödinger equation for $\langle\Psi_K|$ which contains the adjoint Hamiltonian (for a more detailed discussion, see Refs. 21 and 38).

Let us come back to the collision integral (7), where now the scattering rates $\Sigma^{\gtrless}$ are to be given in the T-matrix approximation, and their energy argument is fixed according to the ''on shell'' condition $\hbar\omega = \epsilon_a(p,T) = \epsilon_a^0(p) + \Delta_a(T)$. From Eq. (10), it then follows, after using the Kadanoff-Baym ansatz for $g_b^{\gtrless}$, that

$$i\Sigma_a^{\gtrless}(\mathbf{p}_a,\omega,T)|_{\hbar\omega=\epsilon_a} = \sum_b \int \frac{d\mathbf{p}_b}{(2\pi\hbar)^3}\langle \mathbf{p}_a\mathbf{p}_b|T_{ab}^{\gtrless}(\epsilon_a+\epsilon_b,T)|\mathbf{p}_b\mathbf{p}_a\rangle\, f_b^{\gtrless}(\mathbf{p}_b,T). \tag{14}$$

It turns out that the T matrices $T_{ab}^{\gtrless}$ have to be taken ''on shell,'' too, i.e., their energy argument is $\epsilon_a + \epsilon_b$.[39] This means that only two-particle scattering states contribute to the rates $\Sigma_a^{\gtrless}(\mathbf{p}_a,\epsilon_a)$ for this level of approximation. To include the effect of bound states on the on-shell scattering rates, one has to go beyond the binary collision approximation, taking into account three-body scattering processes between electrons/holes and bound states (e.g., incoherent excitons); see Sec. IV.

For the T matrix in Eq. (14), we find the optical theorem from Eqs. (11) and (12)[38]

$$T_{ab}^{\gtrless}(\omega,T) = 2\pi i\, T_{ab}^{R}(\omega)\, f_a^{\gtrless}(T) f_b^{\gtrless}(T)\, \delta(\hbar\omega - \epsilon_a - \epsilon_b) T_{ab}^{A}(\omega), \tag{15}$$

where $T_{ab}^{R/A}$ are the retarded and advanced T matrices which obey the Lippmann-Schwinger equation (we drop the time argument)

$$T_{ab}^{R/A}(\omega) = V_{ab}^{S} + V_{ab}^{S}\frac{1 - f_a - f_b}{\hbar\omega - \epsilon_a - \epsilon_b \pm i\varepsilon}\, T_{ab}^{R/A}(\omega). \tag{16}$$

If this equation is solved by iteration, a ladder-type diagram expansion follows. In lowest order (neglecting the second term on the right-hand side), the T matrix reduces to the quasistatic interaction potential V^S, which is just the Born approximation discussed in Sec. II A. The retarded T matrix is directly related to the scattering-out state $|\Psi_K\rangle = |\overline{\mathbf{p}}_a\overline{\mathbf{p}}_b +\rangle$, determined by Eq. (13)

$$\langle \mathbf{p}_a\mathbf{p}_b|T_{ab}^{R}(\epsilon_a+\epsilon_b)|\overline{\mathbf{p}}_b\overline{\mathbf{p}}_a\rangle = \langle \mathbf{p}_a\mathbf{p}_b|V_{ab}^{S}|\overline{\mathbf{p}}_b\overline{\mathbf{p}}_a +\rangle. \tag{17}$$

Finally, inserting Eq. (15) into Eq. (14), we can express the scattering rates in binary collision approximation in terms of the retarded T matrix:

$$i\Sigma_a^{\gtrless}(\mathbf{p}_a,\epsilon_a,T)=\frac{1}{V\hbar}\sum_b\int\frac{d\mathbf{p}_b}{(2\pi\hbar)^3}\frac{d\overline{\mathbf{p}}_a}{(2\pi\hbar)^3}\frac{d\overline{\mathbf{p}}_b}{(2\pi\hbar)^3}2\pi\delta(\epsilon_a+\epsilon_b-\overline{\epsilon}_a-\overline{\epsilon}_b)$$
$$\times|\langle\mathbf{p}_a\mathbf{p}_b|T_{ab}^R(\epsilon_a+\epsilon_b)|\overline{\mathbf{p}}_b\overline{\mathbf{p}}_a\rangle|^2 f_a^{\gtrless}(\overline{\mathbf{p}}_a,T)f_b^{\gtrless}(\overline{\mathbf{p}}_b,T)f_b^{\lessgtr}(\mathbf{p}_b,T). \tag{18}$$

Thus, for an evaluation of the scattering rates (18), the central problem is the determination of the retarded T matrix. One approach is to solve the Lippmann-Schwinger equation (16). On the other hand, for nondegenerate plasmas, the T matrix can be determined more efficiently from the solution of the effective Schrödinger equation (13) using scattering phase-shift techniques.

C. Evaluation of the *T*-matrix scattering rates for bulk semiconductors

In the following, we consider nondegenerate *e-h* plasmas. Furthermore, the momentum distributions are assumed isotropic, i.e., $f(\mathbf{p},T)=f(p,T)$, and the interaction is screened quasistatically; see Eq. (9). Transforming Eq. (18) to relative and center-of-mass momenta $\mathbf{p}=(m_b\mathbf{p}_a-m_a\mathbf{p}_b)/(m_a+m_b)$ and $\mathbf{P}=\mathbf{p}_a+\mathbf{p}_b$, the T-matrix approximation can be expressed by the T matrix of the relative motion $\langle\mathbf{p}|T_{ab}^R|\overline{\mathbf{p}}\rangle$.[26] Carrying out the integration over $\mathbf{P}$, we obtain for the scattering rates

$$i\Sigma_a^{<}(\mathbf{p}_a\epsilon_a,T)=\frac{4\pi}{\hbar}\sum_b\frac{m_b^3}{m_{ab}^2}\int\frac{d\mathbf{p}\quad d\overline{\mathbf{p}}}{(2\pi\hbar)^3(2\pi\hbar)^3}|\langle\mathbf{p}|T_{ab}^R|\overline{\mathbf{p}}\rangle|^2\frac{1}{p}\delta(p-\overline{p})f_a(\mathbf{p}_a+\overline{\mathbf{p}}-\mathbf{p},T)\,f_b(\gamma\mathbf{p}_a-\gamma\mathbf{p}-\overline{\mathbf{p}},T), \tag{19}$$

$$i\Sigma_a^{>}(\mathbf{p}_a\epsilon_a,T)=\frac{4\pi}{\hbar}\sum_b\frac{m_b^3}{m_{ab}^2}\int\frac{d\mathbf{p}\quad d\overline{\mathbf{p}}}{(2\pi\hbar)^3(2\pi\hbar)^3}|\langle\mathbf{p}|T_{ab}^R|\overline{\mathbf{p}}\rangle|^2\frac{1}{p}\delta(p-\overline{p})f_b(\gamma\mathbf{p}_a-(1+\gamma)\mathbf{p},T), \tag{20}$$

where $\gamma=m_b/m_a$ is the mass ratio, and $m_{ab}=m_am_b/(m_a+m_b)$ is the reduced mass.

For the further derivations, we express the T matrix by the differential scattering cross section $|\langle\mathbf{p}|T_{ab}^R|\overline{\mathbf{p}}\rangle|^2_{p=\overline{p}}=(2\pi\hbar)^{-6}(2\pi)^{-4}\hbar^{-2}m_{ab}^{-2}\,d\sigma_{ab}(p,\Omega)/d\Omega$. Due to the isotropy of the distribution functions, two integrations can be performed in Eqs. (19) and (20), yielding

$$i\Sigma_a^{<}(p_a\epsilon_a,T)=\frac{4\pi}{(2\pi\hbar)^3}\sum_b\frac{m_b^3}{m_{ab}^4}\int_0^\infty dp\int_{-1}^1 dx_1\int_{-1}^1 dx\int_0^{2\pi}d\varphi_x p^3\frac{d\sigma_{ab}(p,\Omega)}{d\Omega}f_a(p_a^2+2p^2-2\,p_a\,p\,x_1+2\,p_a\,p\,x_2,T)$$
$$\times f_b(\gamma^2(p_a^2+p^2-p_a\,p\,x)+2\,\gamma(p^2\,x-p_a\,p\,x_2)+p^2,T), \tag{21}$$

$$i\Sigma_a^{>}(p_a\epsilon_a,T)=\frac{4\pi}{(2\pi\hbar)^3}\sum_b\frac{m_b^3}{m_{ab}^4}\int_0^\infty dp\int_{-1}^1 dx_1\,p^3\,\sigma_{ab}^{\rm tot}(p)f_b(\gamma^2\,p_a^2+(1+\gamma)^2\,p^2-2\,\gamma(1+\gamma)\,p_a\,p\,x_1,T). \tag{22}$$

In the ''scattering-out'' rate $\Sigma^>$, we introduced the total cross section which follows by integrating $d\sigma/d\Omega$ over the solid angle Ω. The abbreviations x and x_1 are connected with the angles between the momenta $\mathbf{p}$, $\overline{\mathbf{p}}$, and $\mathbf{p}_a$; for a definition, see Ref. 26. Expressions (21) and (22) represent generalizations of the equilibrium T-matrix scattering rates to nonequilibrium electron-hole plasmas. Time dependencies enter the rates via the nonequilibrium momentum distribution functions and the scattering cross section [via the quasistatic potential $V^S(T)$].

In thermodynamic equilibrium, the scattering rates are related via the well-known detailed balance relation

$$\Sigma_a^{<}(p_a,\epsilon_a)=\Sigma_a^{>}(p_a,\epsilon_a)\,f_a^0(p_a), \tag{23}$$

where $f_a^0(p)=n_a\Lambda_a^3/(2s_a+1)\exp(-p^2/2m_ak_BT)$ is the Maxwell distribution function, and the thermal wavelength Λ_a has been defined in Eq. (3). Therefore, in equilibrium, it is sufficient to compute the scattering-out rate given by

$$i\Sigma_a^{>}(p_a,\epsilon_a)=\frac{4\pi}{(2\pi\hbar)^3}\sum_b\frac{m_b^2m_a}{m_{ab}^3}\frac{n_b\Lambda_b^3k_BT}{p_a}\int_0^\infty dp\,p^2\,\sigma^{\rm tot}(p)$$
$$\times\{\exp[-(p_a/m_a-p/m_{ab})^2m_b/2k_BT]-\exp[-(p_a/m_a+p/m_{ab})^2m_b/2k_BT]\}. \tag{24}$$

Expressions (21), (22), and (24) enable us to study the effect of strong correlations in a broad class of equilibrium and nonequilibrium situations, thereby allowing for an efficient numerical evaluation.

III. NUMERICAL RESULTS FOR THE *T*-MATRIX SCATTERING AND DEPHASING RATES IN BULK GALLIUM ARSENIDE

A. Scattering cross sections

As we have seen above, in the scattering rates, the central quantities are the scattering cross sections which are related to the two-particle T matrix. Therefore, we turn to the evaluation of the differential cross sections $d\sigma_{ab}/d\Omega$ making use of the concepts of scattering theory.[27,28] Because of the spherical symmetry of the statically screened Coulomb potential, a partial wave expansion of the scattering quantities can be performed. For the differential cross section, it follows that

$$\frac{d\sigma_{ab}}{d\Omega}=\frac{\hbar^2}{p^2}\sum_{l,l'}^{\infty}(2l+1)(2l'+1)\sin\delta_l\sin\delta_{l'}\cos(\delta_l-\delta_{l'})\,P_l(\cos\vartheta)P_{l'}(\cos\vartheta)$$
$$\times\{1+\delta_{a,b}\tfrac{1}{4}[A(l,l')+B(l,l')]+\delta_{a,b}\tfrac{3}{4}[A(l,l')-B(l,l')]\},\tag{25}$$

where l and l' are the angular momentum quantum numbers, ϑ is the angle between $\mathbf{p}$ and $\overline{\mathbf{p}}$ (scattering angle), $P_l(\cos\vartheta)$ are the Legendre polynomials, and δ_l denote the scattering phase shifts. Furthermore, we have introduced the functions $A(l,l')=(-1)^{l+l'}$ and $B(l,l')=(-1)^l+(-1)^{l'}$. In Eq. (25), the second and third terms in curly brackets account for exchange effects in the case of identical particles.

From Eq. (25), the total cross section is obtained as

$$\sigma_{ab}^{\mathrm{tot}}(p)=\frac{4\pi\hbar^2}{p^2}\sum_{l=0}^{\infty}(2l+1)\sin^2\delta_l,\tag{26}$$

where $a\neq b$ while, for identical particles ($a=b$),

$$\sigma_{aa}^{\mathrm{tot}}(p)=\frac{2\pi\hbar^2}{p^2}\sum_{l=0,2,4\ldots}^{\infty}(2l+1)\sin^2\delta_l$$
$$+\frac{6\pi\hbar^2}{p^2}\sum_{l=1,3,5\ldots}^{\infty}(2l+1)\sin^2\delta_l.\tag{27}$$

Thus we have related the cross sections to the scattering phase shifts δ_l. The latter, in turn, are closely related to the two-particle wave function u_l, which obeys the radial Schrödinger equation

$$\left[\frac{\mathrm{d}^2}{\mathrm{d}r^2}-\frac{l(l+1)}{r^2}-\frac{2m_{ab}}{\hbar^2}V_{ab}^S(r)\right]u_l(k,r)=k^2u_l(k,r).\tag{28}$$

Here $k^2=2m_{ab}(\epsilon_{ab}-\Delta_{ab})/\hbar^2$ is the square of the wave number, with $\Delta_{ab}=\Delta_a+\Delta_b$ being the two-particle self-energy correction. The scattering phase shifts can be determined from the asymptotics of the scattering solutions.[28] Assuming a finite interaction range r_0, the continuity condition of the logarithmic derivative of the wave function at the point $r=r_0$ leads to the following expression for the scattering phase shifts:

$$\tan\delta_l(k)=\frac{u_l(kr_0)\,j_l'(kr)-u_l'(kr)\,j_l(kr_0)}{u_l(kr_0)\,n_l'(kr)-u_l'(kr)\,n_l(kr_0)}.\tag{29}$$

The prime denotes the derivative with respect to r at $r=r_0$, and $j_l(z)$, $n_l(z)$ are the Riccati-Bessel functions; see, e.g., Ref. 27.

In order to calculate the phase shifts, the Schrödinger equation (28) has to be solved numerically. We have done this using the Numerov algorithm[40,24] to calculate the wave function and its derivative for a given l up to the point $r=r_0$. This point was chosen such that the ratio of potential and scattering energy dropped sufficiently (below $<10^{-5}$ in our calculations). Knowing the scattering phase shifts, the cross sections are computed according to Eqs. (25)–(27). For a given value of the wave number k, only a limited number of partial waves gives significant contributions to the l sum which, therefore may be truncated for a certain $l=l_0$ (l_0 was chosen such that the contribution of the remaining terms was less than 10^{-5}).

Before presenting numerical results, we briefly summarize the cross sections in the Born approximation, as they will be needed for the numerical comparisons below. The Born approximation follows from the Lippmann-Schwinger equation (16) by taking only the first term, i.e., $T_{ab}^{R/A}\to V_{ab}^S$. For the differential scattering cross section of the e-h scattering, we obtain

$$\frac{d\sigma_{ab}^B(p,\Omega)}{d\Omega}=\left[\frac{2m_{ab}e_ae_b/\epsilon_B}{\hbar^2\kappa^2+4p^2\sin\dfrac{\vartheta}{2}}\right]^2.\tag{30}$$

For completeness, we give the result for identical particles with exchange effects included. Here the cross section is composed of singulet ($+$) and triplet ($-$) contributions according to $d\sigma_{aa}/d\Omega=\frac{1}{4}(d\sigma_{aa}^+/d\Omega)+\frac{3}{4}(d\sigma_{aa}^-/d\Omega)$, where

$$\frac{d\sigma_{aa}^{B\pm}(p,\Omega)}{\mathrm{d}\Omega}=\frac{1}{2}\left[\frac{m_ae_a^2C_\pm(p,\vartheta)/\epsilon_B}{\hbar^4\kappa^4+4\hbar^2\kappa^2p^2+4p^4\sin^2\vartheta}\right]^2,\tag{31}$$

$$C_+(p,\vartheta)=2\hbar^2\kappa^2+4p^2,\quad C_-(p,\vartheta)=4p^2\cos\vartheta.$$

The corresponding results for the total cross section are

$$\sigma_{ab}^{B,\mathrm{tot}}=\frac{16\pi}{a_B^2}\frac{m_{ab}^2}{m_{eh}^2}\left[\frac{\hbar^2}{\kappa^2(\hbar^2\kappa^2+4p^2)}\right.$$
$$\left.+\delta_{ab}\frac{\hbar^4}{8p^2(\hbar^2\kappa^2+2p^2)}\ln\left(4\frac{p^2}{\hbar^2\kappa^2}+1\right)\right],\tag{32}$$

with the exciton Bohr radius $a_B=\hbar^2\epsilon_B/m_{eh}e^2$.

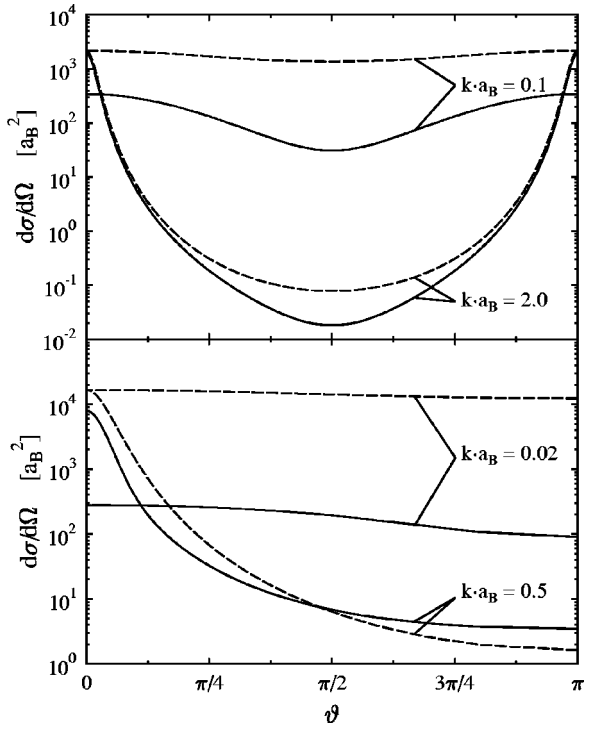

FIG. 2. Differential scattering cross section of the *e*-*e* and *e*-*h* scattering (upper and lower figure, respectively) for two theoretical models: the *T*-matrix (full line) and Born approximations (dashed line). ϑ is the scattering angle. The wave number $k=p/\hbar$ is fixed (shown in the figure), and the screening parameter is $\kappa=0.1\,a_B^{-1}$.

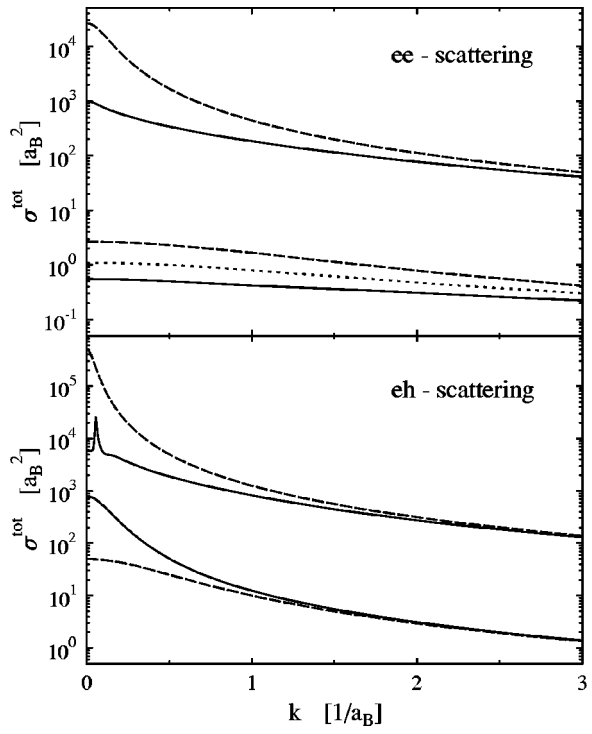

FIG. 3. Total scattering cross sections $\sigma^{\rm tot}$ of the *e*-*e* and *e*-*h* scattering (upper and lower figure, respectively) (*T*-matrix approximation, full line; *T*-matrix approximation without exchange, dotted line; Born approximation, dashed line). The screening parameters are $\kappa=0.1\,a_B^{-1}$ (upper pairs of lines) and $\kappa=1.0\,a_B^{-1}$ (lower triple/pair of lines).

Let us now discuss the numerical results for the scattering cross sections in the *T*-matrix and Born approximations. The cross sections reflect the microscopic properties of the two-particle scattering process, and are thus the basis for the macroscopic behavior. In Fig. 2, the differential scattering cross sections for *e*-*e* and *e*-*h* scattering are plotted versus the scattering angle for two fixed wave numbers $k=p/\hbar$, whereas Fig. 3 shows the momentum dependence of the total cross section.

(i) First, we notice the qualitatively different scattering angle dependence of the differential cross sections for different scattering partners. For *e*-*h* scattering (the lower part of Fig. 2), $d\sigma/d\Omega$ decays monotonically with increasing angle ϑ. In contrast, for identical particles (upper part), the curves increase again for large angles; in fact they are symmetric with respect to $\vartheta=\pi/2$. This behavior is readily explained by quantum-mechanical exchange effects and is, of course, independent of the approximation for the scattering cross section. In particular, it is most clearly seen in the analytical expressions (31) for the Born approximation. Analogous results are observed for the hole-hole scattering (not shown).

(ii) For small *k*, in both Born and *T*-matrix approximations, the cross section changes only weakly as function of the scattering angle (Fig. 2), whereas, for large wave numbers, it increases by several orders of magnitude when approaching the angle $\vartheta=0$ (and, additionally, $\vartheta=\pi$ for identical particles). This is intuitively clear because, with increasing kinetic energy, it becomes more unlikely that a particle is deflected under a large angle.

(iii) The general tendency is that the *T*-matrix cross sections are smaller than the Born approximation results. The largest deviations are observed for small wave numbers *k* (independently of the scattering partners), whereas, for large *k*, the differences vanish. An exception is the *e*-*h* scattering, where for intermediate *k* and large scattering angles, the *T*-matrix results may slightly exceed the Born approximation (for identical particles, this effect is suppressed by the exchange contribution). This explicitly confirms that the Born approximation overestimates small angle and small-*k* scattering, but underestimates larger momentum-transfer processes.

(iv) Although the angle integration smooths out many details of the differential cross section, the main features remain visible in the total scattering cross sections (27) and (26). Again we see that the *T*-matrix cross sections are smaller than the Born approximation, except for the *e*-*h* scattering at $\kappa=1.0\,a_B^{-1}$. The general trend is a monotonic decrease with increasing wave number, except for well-pronounced peaks in the case of *e*-*h* scattering. These peaks are due to two–particle resonances in the continuum of scattering states. They appear when, due to screening, excitonic bound-state levels are shifted into the continuum (Mott effect). Thus these resonances are traces of bound states contributing to the low-energy part of the *T*-matrix cross section. In particular, the peak in Fig. 3 ($\kappa=0.1\,a_B^{-1}$) is due to the $3d$ resonance, whereas the increase of the *T*-matrix *e*-*h* cross section at $\kappa=1.0\,a_B^{-1}$ for low momenta is related to the 1s resonance. For identical particles, exchange effects reduce the cross section, which is noticable at large screening parameters (see curve $\kappa=1.0\,a_B^{-1}$).

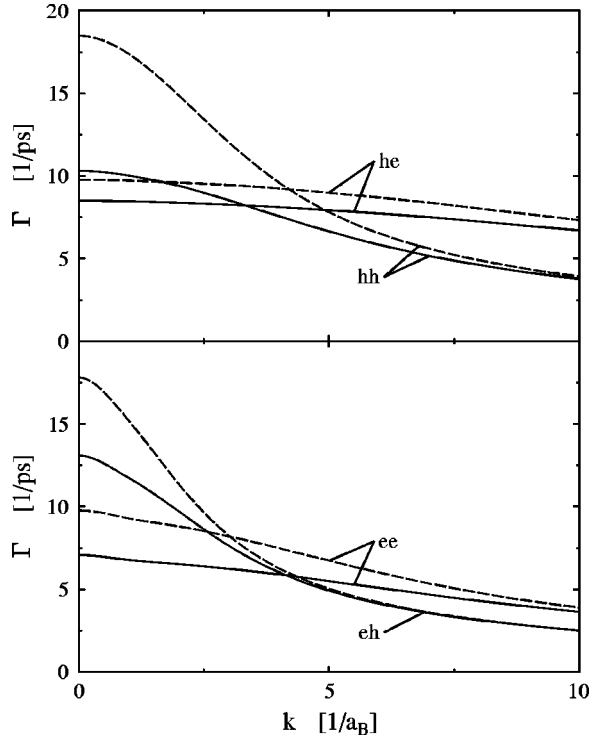

FIG. 4. Equilibrium dephasing rate $\Gamma = i\Sigma^{>} + i\Sigma^{<}$ for different scattering processes vs the wave number. The curves correspond to the *T*-matrix approach (full lines) and the Born approximation (dashed lines). The density is $n = 10^{16}$ cm^{-3}, and the temperature $T = 300$ K.

B. Equilibrium *e-e*, *e-h*, and *h-h* scattering rates

Now we turn to the scattering rates, beginning with an analysis of the equilibrium case. Here, only the total cross section $\sigma_{ab}^{\mathrm{tot}}$ is needed, cf. Eq. (24). First we discuss the behavior of the dephasing rates $\Gamma_a = i\Sigma_a^{>} + i\Sigma_a^{<}$ as a function of the wave number. In Fig. 4, the four different scattering processes in the *e-h* plasma are compared at room temperature and $n = 10^{16}\,\mathrm{cm}^{-3}$. As for the total cross section [see point (iv) above], the largest deviations between the *T*-matrix and Born approximations occur for small momenta. For increasing wave number, the deviations vanish quickly for *h-h* and *e-h* scattering, but persist much longer for *e-e* and *h-e* scattering. This is a simple mass effect which is readily seen from Eq. (24). The first exponent in brackets has its maximum at $p = [m_b/(m_a + m_b)]p_a$. Therefore, for $b = e$ (for any given p_a), smaller momenta p (where σ^{tot} is large and deviates stronger from the Born approximation) contribute more than in the case $b = h$. For the same reason, the *e-e* and *h-e* dephasing rates decay much more weakly with the wave number, and exceed the *e-h* and *h-h* scattering for sufficiently large *k*.

The temperature dependence is explored for a lower density over a larger range in Fig. 5, where the ratio of the *T*-matrix and Born approximation scattering rates ($\Sigma_{ee}^{>}$ and $\Sigma_{eh}^{>}$), which dominate the behavior of the dephasing rates at low densities, is plotted. Again we see that for increasing wave number the deviations are generally smaller, and they further decrease with increasing temperature. On the other hand, at low temperatures, the ratio of the *e-h* scattering

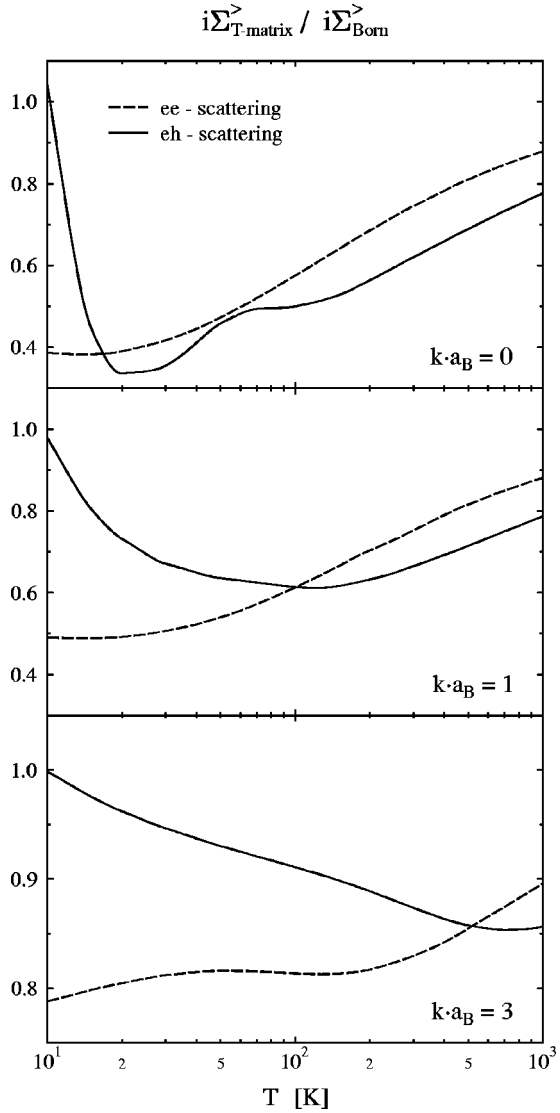

FIG. 5. Ratio of the scattering rates in the *T*-matrix and Born approximations ($\Sigma_{ee}^{>}$, dashed lines; $\Sigma_{eh}^{>}$, solid lines) vs the temperature *T* for three different wave numbers $k = p/\hbar$ (shown in the figure). The carrier density is $n = 10^{15}$ cm^{-3}.

rates is dominated by resonances which are clearly visible even on the macroscopic level of the scattering rates: the shoulder in the upper Fig. 5 around $T = 60$ K is due to the $2s$ and $2p$ resonances, whereas the strong low-temperature rise comes from the $1s$ resonance (cf. also Fig. 3). A discussion of the density dependence of the scattering rates can be found in Ref. 26 and also in Sec. IV B, where we will consider the effect of dynamical screening, see also Fig. 9.

So far we considered the situation of GaAs. To obtain at least a qualitative picture of the magnitude of strong-coupling effects in other bulk materials, in Fig. 6 we show results for three different mass ratios m_h/m_e (for the sake of comparison, the Bohr radius and the binding energy were left constant). The general trend is clear: *T*-matrix effects become more important for increasing mass ratios. While the *e-e* and *h-e* scattering rates change only weakly, there is a substantial reduction of the *T*-matrix rates for *e-h* scattering, and an even stronger one for *h-h* scattering.

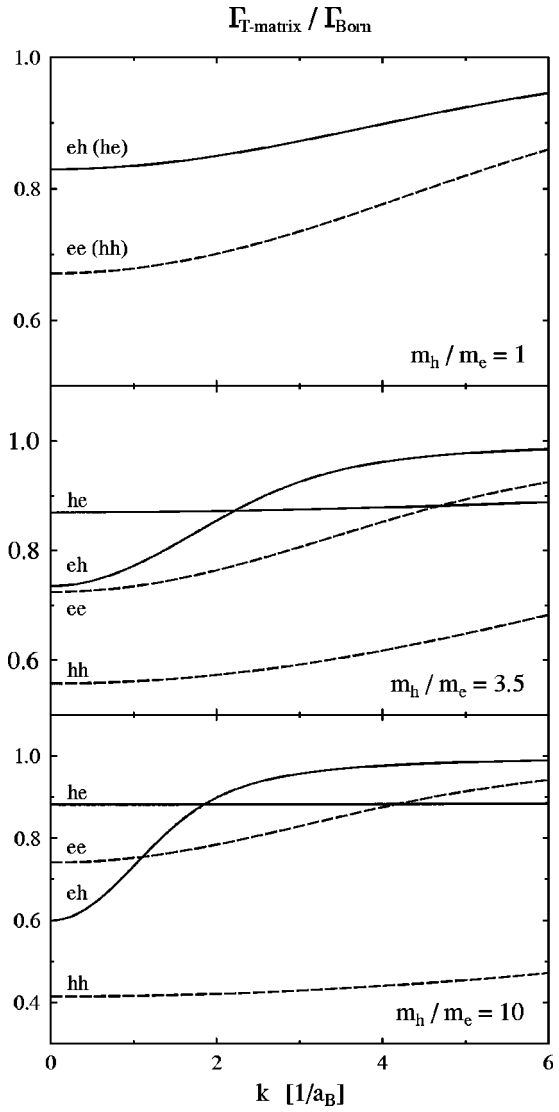

FIG. 6. Ratio of the dephasing rates in the *T*-matrix and Born approximations for different scattering processes and three different hole-electron mass ratios (shown in the figure) vs the wave number. The carrier density is $n=10^{16}$ cm^{-3}, and the temperature $T=300$ K.

C. Strong-coupling effects in nonequilibrium

We now turn to a discussion of strong-coupling effects under nonequilibrium conditions. In particular, we are interested to see if there exist special excitation conditions of the electron-hole plasma which would enhance the difference between the Born and *T*-matrix approximations. To this end, we now have to consider the nonequilibrium formulas for the scattering rates [Eqs. (21) and (22)]. Notice that the expression for $\Sigma^<$ contains a fourfold integral which makes the evaluation of the nonequilibrium *T*-matrix scattering rates rather time consuming. We have performed a series of scattering rate calculations for various nonequilibrium distributions as they are generated, e.g., under typical optical excitation conditions. To simulate different photon energies and pulse durations, we used Gaussian carrier distributions $f(p)=A\exp[(p/\hbar-k_0)^2/\gamma]$ with a different peak momentum $\hbar k_0$ and width γ; see Figs. 7 and 8.

In Fig. 7, we compare the scattering rates for a localized and a very broad distribution ($f_e=f_h$), both centered around

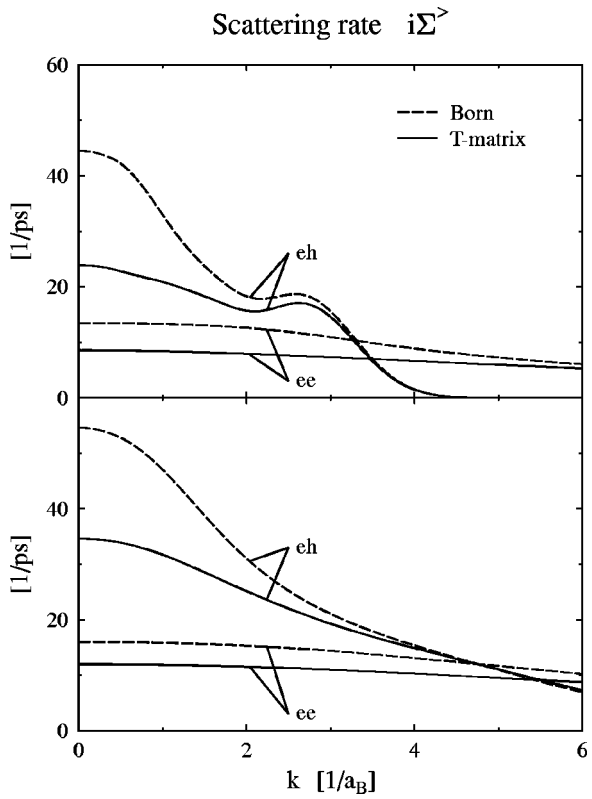

FIG. 7. Electron dephasing rates for two different nonequilibrium situations: upper part, localized Gaussian distribution ($k_0=2.5\,a_B^{-1}, \gamma=0.5\,a_B^{-2}$); lower part, broad Gaussian distribution ($\gamma=2.5\,a_B^{-2}$). *T*-matrix and Born results are plotted as solid and dashed lines, respectively. The carrier distributions correspond to a density of $n=5\times10^{15}$ cm^{-3}.

the same peak momentum and corresponding to the same carrier density of 5×10^{15} cm^{-3}. Despite the different shape of the distributions, the qualitative picture in the two cases is the same: The relative role of the *T*-matrix effects is larger for *e*-*h* scattering than for *e*-*e* scattering, although for the latter the effect is seen up to larger momenta. The absolute magnitude of the effect is higher for the localized distribution. Here the Born approximation is up to 90% higher (*e*-*h* scattering, zero momentum) than the *T*-matrix approximation, compared to about 60% for the broad distribution.

The situation is more complex in Fig. 8, which shows calculations for varying peak positions of the nonequilibrium distribution, while its width and density have been kept constant. From the bottom to the center figure, the deviation of the Born approximation dephasing rate above the *T*-matrix level increases from a factor of about 1.5 to almost 2 at zero momentum, which seems to confirm the trend of Fig. 7. However, a further shift of the carrier distribution toward the band edge (upper figure) gives rise to the opposite trend. The *T*-matrix dephasing rates become even larger than the Born result for low momenta. To understand the reason for this behavior, we plot the electron-scattering rates $\Sigma^>$ in the left column, broken down into *e*-*e* and *e*-*h* contributions. Clearly, the relative growth of the *T*-matrix rates comes from the electron-hole scattering, which is quite similar to the behavior which we observed previously in the equilibrium case at low temperatures (see Fig. 5). In fact, the value of the inverse screening length κ is slightly above the Mott point,

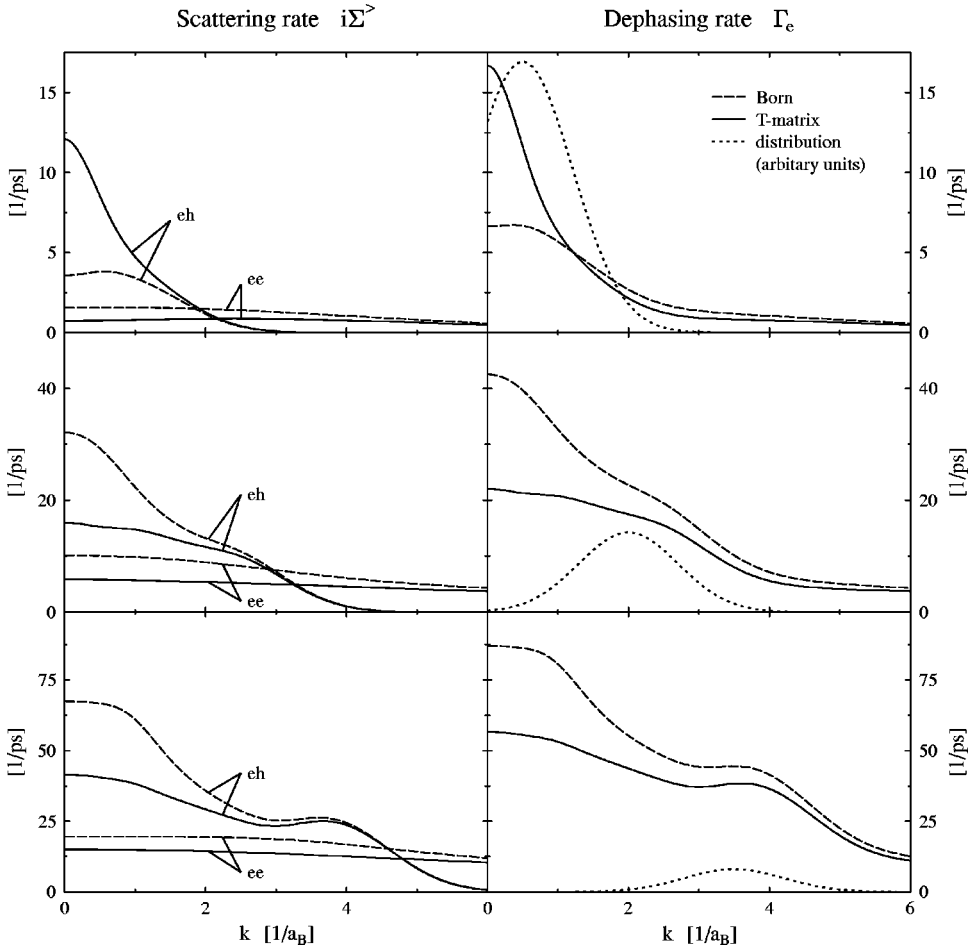

FIG. 8. Electron-scattering rates (left) and dephasing rates (right) for three nonequilibrium distributions, $f_e(k)=f_h(k)$, shown in the figure (dotted lines). The carrier density is $n=5\times10^{15}$ cm^{-3}. *T*-matrix and Born results are plotted as solid and dashed lines, respectively.

i.e., this behavior is again caused by the *s*-wave resonance, which here is observed under nonenquilibrium conditions.

With expressions (21) and (22), inserted into the collision integral (7), time-dependent solutions of the coupled kinetic equations for the electron and hole distributions have been performed, starting with initial distributions of the above type. We found that using the *T*-matrix approximation does not strongly change the shape of the distributions, but generally slows down the relaxation compared to the Born approximation.

Summarizing the effect of nonequilibrium carrier distributions, we have observed quite substantial strong collision effects. The magnitude and sign of the effect depend strongly on the shape of the distribution and on the carrier density. In most cases, the Born approximation overestimates the total scattering and dephasing rates. The largest deviations are predicted for distributions which are localized in momentum space. Furthermore, the deviations are particularly large at low momenta, and may reach 100% and more. On the other hand, in situations slightly above the Mott point, where the 1*s* exciton state is still visible as a resonance, we observe a strong enhancement of the nonequilibrium *T*-matrix scattering rates. This is found, for the given density, for distributions which are localized at low momenta.

IV. DISCUSSION

A. Limitations of the theory

Let us now discuss the range of validity of the presented results. To make a numerical evaluation of the *T*-matrix approximation possible, it was necessary to introduce simplifications. First of all, the effect of dynamical screening had to be neglected, cf. Eqs. (11) and (13); we come back to this question below. Second, we neglected degeneracy effects, which limits our results to parameters below the dashed line in Fig. 1. To estimate the relevance of these effects, we plotted the static Born approximation results with full Pauli blocking included in Fig. 9 (dash-dotted line). As anticipated, the effect is a reduction of the scattering rates which sets in around $n=10^{16}$ cm^{-3}. It is reasonable to expect an

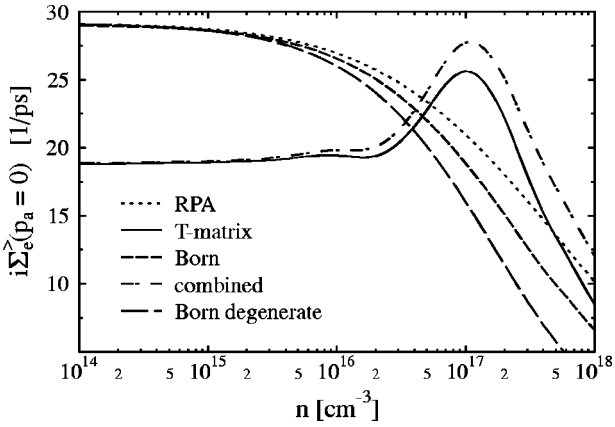

FIG. 9. Electron-scattering rate $\Sigma_e^>=\Sigma_{ee}^>+\Sigma_{eh}^>$ as a function of the carrier density for a momentum $p_a=0$ and a temperature $T=300$ K for different theoretical models.

analogous influence on the *T*-matrix results, because at high densities both approximations should merge as in the case without degeneracy effects.

The third limitation results from a neglect of bound states, in particular (incoherent, as opposed to the interband polarization) excitons. It is, of course, well known how to incorporate bound states into the on-shell scattering rates: One has to include three-body scattering processes between a free carrier and a bound *e*-*h* pair. This requires a kinetic equation for excitons, which has to be solved simultaneously, which is not yet feasible. However, for the parameters considered in the present study, the effect of incoherent excitons is found to be small. This can be verified by estimating the fraction α_B of electrons bound in excitons, e.g., from a mass action law or coupled rate equations.[41] We solved a mass action law (Saha equation) using an effective exciton binding energy $E_B^{\rm eff}=E_B^0+\Delta I$, where $E_B^0=4.2$ meV (GaAs), and the lowering of the ionization energy is due to screening and self-energy effects, $\Delta I=-\kappa e^2/\epsilon_B$. We found that, for temperatures above 50 K, over the whole density range, α_B does not exceed 20%, which justifies our approach. Of course, at lower temperature, excitonic effects will be important.

B. Dynamical screening effects in the *T*-matrix approximation

Further improvement of the theory of carrier–carrier scattering requires the inclusion of dynamical screening into the *T*-matrix approximation. This can be done, e.g., in the framework of the dynamically screened ladder approximation of Green's functions theory[21] which, in nonequilibrium, is out of reach. Alternatively, one can try to incorporate dynamical screening into our approach approximately. To this end, we use a combination of static *T*-matrix (''T''), static (''B'') and dynamically screened Born approximations (''RPA'') for the self-energies[42] (see also Refs. 43 and 44)

$$\Sigma_a=\Sigma_a^{\rm T}+\Sigma_a^{\rm RPA}-\Sigma_a^{\rm B}. \tag{33}$$

In a nondegenerate equilibrium *e*-*h* plasma, the RPA scattering-out rate [Eq. (8)] simplifies to

$$i\Sigma_a^{>}(p_a\epsilon_a)=-\frac{2e^2m_a}{\pi\hbar\, p_a}\int_0^\infty\frac{dp}{p}\int_{-(p^2/2m_a)-(p\,p_a/m_a)}^{-(p^2/2m_a)+(p\,p_a/m_a)}d\omega\,{\rm Im}\,\epsilon^{R-1}(p,\omega)n_B(\omega), \tag{34}$$

where the Bose function $n_B(\omega)=[\exp(\omega/k_BT)-1]^{-1}$ represents the plasmon distribution. In Fig. 9, we show the simultaneous effect of dynamical screening and strong correlations for the electron-scattering rate $\Sigma_e^>$ at zero momentum as a function of density. One clearly sees that the combined model (33) yields the correct limits: at low densities (below 10^{16} cm^{-3}), it practically coincides with the static *T* matrix, whereas for high densities, it approaches the RPA. In between, the combined scheme essentially follows the static *T*-matrix behavior, with the dynamics leading to a slight overall increase.

According to Fig. 1, we expect correlation effects to vanish beyond $n\sim10^{18}$ cm^{-3}. This is indeed observed in Fig. 9, as Born and *T*-matrix results merge at high densities. This trend is interrupted only for the *e*-*h* scattering (see Ref. 26) which is again a consequence of resonances giving rise to the shoulder around $n=10^{16}$ cm^{-3}($2s/2p$ resonances) and the peak aroud $n=10^{17}$ cm^{-3} (1s). However, for low densities, we do not observe a merging of the Born and *T*-matrix results, clearly indicating the breakdown of the former. The reason for this is that, due to the decrease of screening, *T*-matrix effects remain important at low densities as well.

Finally, let us consider the effect of dynamical screening for different particle momenta. Figure 10 shows the electron dephasing rate Γ_e for $n=10^{15}$ cm^{-3} and $T=300$ K, and the same approximations as above as a function of wave number. Clearly, for small wave numbers, dynamical screening effects are small while strong correlations are dominant. Consequently, the static *T*-matrix approximation and the combined scheme are close to each other. In contrast, for large wave numbers, static *T*-matrix and Born approximations merge. In this case, the dynamical screening effects are essential, and the combined scheme is governed by the RPA contribution. For intermediate wave numbers, the combined scheme smoothly interpolates between the two limiting cases.

C. Summary

In this paper, a treatment of carrier-carrier scattering in semiconductors was presented which goes beyond the common Born approximation. It was shown theoretically and numerically that the Born approximation strongly overestimates small-angle scattering, but cannot describe the effect of strong collisions. This becomes a serious problem if the coupling parameter Γ is of the order of 1 or larger, i.e., in the corner of correlations (see Fig. 1). However, the Born ap-

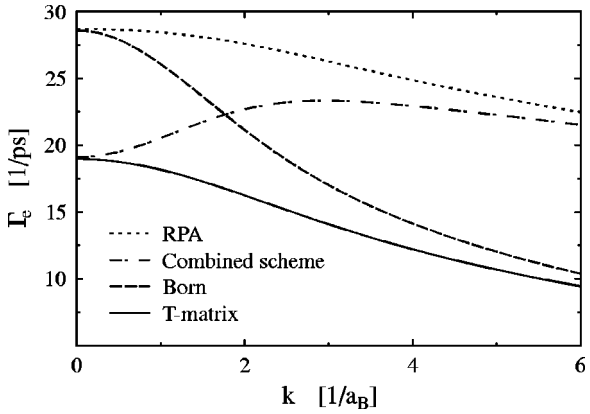

FIG. 10. Electron dephasing rate $\Gamma_e=\Gamma_{ee}+\Gamma_{eh}$ as a function of the wave number for a density $n=10^{15}$ cm^{-3} and a temperature $T=300$ K for different approximations.

proximation fails not only in the ''corner of correlations'' but also at low densities, where only the *T*-matrix approximation reproduces the correct analytical limits. We have shown that deviations of the Born approximation from the more general *T*-matrix result are visible not only in the microscopic scattering quantities (cross sections), but also in macroscopic quantities, such as scattering and dephasing rates. There the Born approximation results may be wrong by as much as a factor of 2 and more, leading, in most cases, to rates that are too high. Similar behavior should be expected for other transport coeffecients and for optical properties.

ACKNOWLEDGMENTS

This work was supported by the Deutsche Forschungsgemeinschaft (Schwerpunkt ''Quantenkohärenz in Halbleitern'' and SFB 198 ''Kinetik partiell ionisierter Plasmen'') and by a grant for CPU time at the HLRZ Jülich.

[1] For a review, see, e.g. J. Shah, Solid-State Electron. **32**, 1051 (1989).
[2] A. Alexandrou, V. Berger, and D. Hulin, Phys. Rev. B **52**, 4654 (1995).
[3] A. Leitenstorfer, C. Fürst, A. Laubereau, and W. Kaiser, Phys. Rev. Lett. **76**, 1545 (1996).
[4] H. Haug and A. P. Jauho, *Quantum Kinetics in Transport and Optics of Semiconductors* (Springer-Verlag, Heidelberg, 1996).
[5] D. C. Scott, R. Binder, and S. W. Koch, Phys. Rev. Lett. **69**, 347 (1992).
[6] R. Binder, D. Scott, A. E. Paul, M. Lindberg, K. Henneberger, and S. W. Koch, Phys. Rev. B **45**, 1107 (1992).
[7] J. H. Collet, Phys. Rev. B **47**, 10 279 (1993).
[8] M. Lindberg and S. W. Koch, Phys. Rev. B **38**, 3342 (1988).
[9] For a review, see, e.g., R. Binder and S. W. Koch, Prog. Quantum Electron. **19**, 307 (1995).
[10] M. Bonitz and D. Kremp, Phys. Lett. A **212**, 83 (1996).
[11] K. El Sayed, S. Schuster, H. Haug, F. Herzel, and K. Henneberger, Phys. Rev. B **49**, 7337 (1994).
[12] K. El Sayed, L. Banyai, and H. Haug, Phys. Rev. B **50**, 1541 (1994).
[13] D. B. Tran Thoai and H. Haug, Z. Phys. B **91**, 199 (1993).
[14] W. Schäfer, J. Opt. Soc. Am. B **13**, 1291 (1996).
[15] M. Bonitz, D. Kremp, D. C. Scott, R. Binder, W. D. Kraeft, and H. S. Köhler, J. Phys.: Condens. Matter **8**, 6057 (1996).
[16] We mention that *T*-matrix effects have been intensively studied in semiconductor transport in application to impurity scattering; for an overview, see *Quantum Kinetics in Transport and Optics of Semiconductors* (Ref. 4).
[17] In field-dependent truncation schemes, strong-coupling effects are included. See, e.g., V. M. Axt and A. Stahl, Z. Phys. B **93**, 195 (1994). However, this approach is limited to weak optical fields.
[18] Indications of overly high scattering rates in the Born approximation in two-dimensional *e*-*h* plasmas were given by M. Mosko, A. Moskova, and V. Cambel, Phys. Rev. B **51**, 16 860 (1995).
[19] P. Danielewicz, Ann. Phys. (N.Y.) **197**, 154 (1990).
[20] W. Ebeling, W. D. Kraeft, and D. Kremp, *Theory of Bound States and Ionization Equilibrium in Plasmas and Solids* (Akademie-Verlag, Berlin, 1976).
[21] W. D. Kraeft, D. Kremp, W. Ebeling, and G. Röpke *Quantum Statistics of Charged Particle Systems* (Akademie-Verlag, Berlin, 1986).
[22] H. Stolz, *Einführung in die Vielelektronentheorie der Kristalle* (Akademieverlag, Berlin, 1974).
[23] W. Schäfer and J. Treusch, Z. Phys. B **63**, 407 (1986).
[24] R. Zimmermann, *Many-Particle Theory of Highly Excited Semiconductors* (Teubner, Leipzig, 1987).
[25] L. P. Kadanoff and G. Baym, *Quantum Statistical Mechanics* (Benjamin, New York, 1962).
[26] D. O. Gericke, S. Kosse, M. Schlanges, and M. Bonitz, Phys. Status Solidi B **206**, 257 (1998).
[27] R. G. Newton *Scattering Theory of Waves and Particles* (Springer-Verlag, Berlin, 1982).
[28] J. R. Taylor *The Quantum Theory of Nonrelativistic Collisions* (Wiley, New York, 1972).
[29] R. Schepe, T. Schmielau, D. Tamme, and K. Henneberger, Phys. Status Solidi B **206**, 273 (1998).
[30] N. H. Kwong, M. Bonitz, R. Binder, and S. Köhler, Phys. Status Solidi B **206**, 197 (1998).
[31] For improved solutions which account for non-Markovian effects, we refer to Ref. 32, and for its extention to multiband systems to Ref. 33.
[32] P. Lipavsky, V. Spicka, and B. Velicky, Phys. Rev. B **34**, 6933 (1986).
[33] H. Haug, Phys. Status Solidi B **173**, 139 (1992).
[34] H. Haug and S. W. Koch, *Quantum Theory of the Optical and Electronic Properties of Semiconductors* (World Scientific, Singapore, 1993).
[35] F. Jahnke, M. Kira, S. W. Koch, G. Khitrova, E. K. Lindmark, T. R. Nelson, D. V. Wick, J. D. Berger, O. Lyngnes, H. M. Gibbs, and K. Tai, Phys. Rev. Lett. **77**, 5257 (1996).
[36] P. Danielewicz, Ann. Phys. (N.Y.) **152**, 239 (1984).
[37] D. Kremp, M. Schlanges, and Th. Bornath, J. Stat. Phys. **41**, 661 (1985).
[38] Th. Bornath, D. Kremp, W. D. Kraeft, and M. Schlanges, Phys. Rev. E **54**, 3274 (1996).
[39] This is verified by considering Eq. (12) for the argument $\hbar\omega = \epsilon_a + \epsilon_b$ (scattering state). The δ function confines the sum to scattering state contributions with $E_K = \epsilon_a + \epsilon_b$. Only these frequency arguments appear in the scattering rates (14).
[40] B. Numerov, Publ. Observ. Astrophys. Centr. Russie 11, Moskau (1923).
[41] D. Kremp, M. Schlanges, and Th. Bornath, Phys. Status Solidi B **147**, 747 (1988).
[42] H. A. Gould and H. E. DeWitt, Phys. Rev. **155**, 68 (1967).
[43] F. Morales, M. K. Kilimann, R. Redmer, M. Schlanges, and F. Bialas, Contrib. Plasma Phys. **29**, 425 (1989).
[44] D. O. Gericke, M. Schlanges, and W. D. Kraeft, Phys. Lett. A **222**, 241 (1996).